Electronic Supplementary Material (ESI) for CrystEngComm.

Formation of multi-component crystals with a series of pyridinium-carboxyacrylate zwitterions

Jean Lombard, Leigh Loots, Tanya le Roex and Delia A. Haynes*

Department of Chemistry and Polymer Science, Stellenbosch University, P. Bag X1, Matieland, 7602, Republic of South Africa.

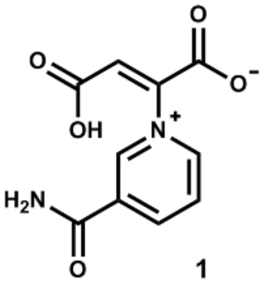

1

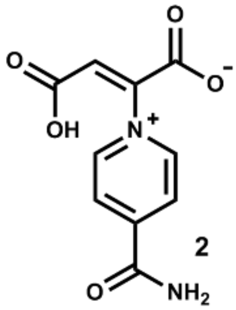

2

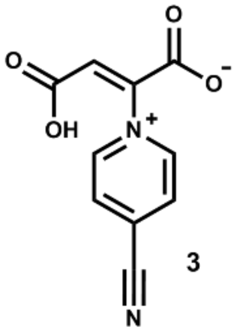

3

Further details regarding synthesis and crystallisation attempts

All chemicals and solvents were obtained from Sigma Aldrich South Africa and used without further purification. Full details regarding the successful synthesis of **1**, **2**, **2a**¸ **1•Melamine**, **2•Melamine** and **3•Melamine** are given in the experimental section of the paper.

Synthesis and crystallisation of zwitterions involved mixing ~0.175 mmol acetylenedicarboxylic acid (ADC) with one equivalent of the respective pyridine derivative in less than 10 ml of solvent or solvent mixture, followed by heating.

Various solvent mixtures were used to synthesise zwitterion **1**: combinations of methanol, ethanol, water, dimethylformamide and dimethylsulfoxide with each other as well as with acetone, acetonitrile, chloroform, dichloromethane, diethyl ether, 1,4-dioxane, tetrahydrofuran, toluene, cyclohexane, ethyl acetate and benzene (a total of 70 different combinations). All of these produced the zwitterion (whether a powder or crystals) and no salts, polymorphs or solvates were ever observed.

A similar procedure was followed for zwitterion **2**. Crystallisation led to the salt **2a** forming initially, but no solvates or polymorphs were observed.

Various co-formers other than those discussed in the paper (melamine, aminopyridine, diaminopyridine) were combined with zwitterions **1**-**3**, but no other multi-component crystals were formed. The co-formers used included: urea, isonicotinamide, nicotinamide, uracil, terephthalic acid, DABCO, 2-aminopyrimidine, thymine, pyrogallol, 2,2'-biphenol, isoquinoline, pyridine, 4-methylphenol, 2,3-dihydroxynaphthalene, naphthalene, phloroglucinol dihydrate, N-phenyl-2-naphthylamine, pamoic acid, hydroquinone, piperazine, pyrazinecarboxylic acid, 4-phenylpyridine, 4-hydroxybenzaldehyde, α,α'-dibromo-o-xylene, and 2-aminobenzonitrile.

Formation of multi-component crystals was attempted by grinding ~0.042 mmol of each zwitterion with one equivalent of the respective co-former, with a few drops of methanol, for 10 minutes using a mortar and pestle. Experiments were then repeated using a few drops of THF instead of methanol. Formation of multi-component crystals was also attempted in solution, on the same scale, by dissolving a 1:1 molar ratio of zwitterion and co-former in water, and stirring them together at 100 °C until the components had completely dissolved. The vials were capped and left on a shelf to allow crystallisation at room temperature.

We also attempted to co-crystallise the zwitterions with each other, in the same way, *via* both mechanochemical and solution methods. Mechanochemical combination of the zwitterions simply lead to physical mixtures of zwitterions, while solution crystallisations lead to the zwitterions crystallising out separately.

Characterisation methods

Powder X-ray diffraction (PXRD) patterns were collected on a Bruker D2 Phaser powder X-ray diffractometer equipped with a copper source producing radiation of wavelength 1.54183 Å. The instrument was operated at 30 kV voltage and 10 mA current. Samples were gently crushed and flattened onto a zero-background holder. Each scan was made up of 2260 steps of 0.5 seconds each (0.0161° step size) that ranged from $2\theta = 4$ to 40°.

Thermogravimetric analysis (TGA) was carried out using a TA Q500 instrument. Powdered samples (3-15 mg) were suspended in an open aluminium pan while being heated in a furnace at 10 °C min^{-1}. The sample was kept under the flow of nitrogen gas throughout (50 ml min^{-1}) to ensure that solvent vapours and decomposition materials were removed as they formed.

Differential Scanning Calorimetry (DSC) was carried out using a TA Q20 instrument. Powdered samples (3-10 mg) were placed in a closed aluminium pan. The lid of the pan was punctured before closing. An empty reference pan was prepared in the same way. Both pans were placed under a nitrogen flow of 50 ml min^{-1} and heated at 10 °C min^{-1} until just before decomposition.

Nuclear Magnetic Resonance (NMR) spectroscopy was performed using a 300 MHz Agilent spectrometer. Samples were dissolved in D_2O and filtered before analysis. Where needed, a few drops of pyridine were added to aid dissolution. Fourier Transform Infrared spectroscopy (FTIR) was carried out using a Bruker Alpha spectrometer with Platinum ATR attachment. A background scan was acquired before each sample scan.

Powder X-Ray diffraction patterns

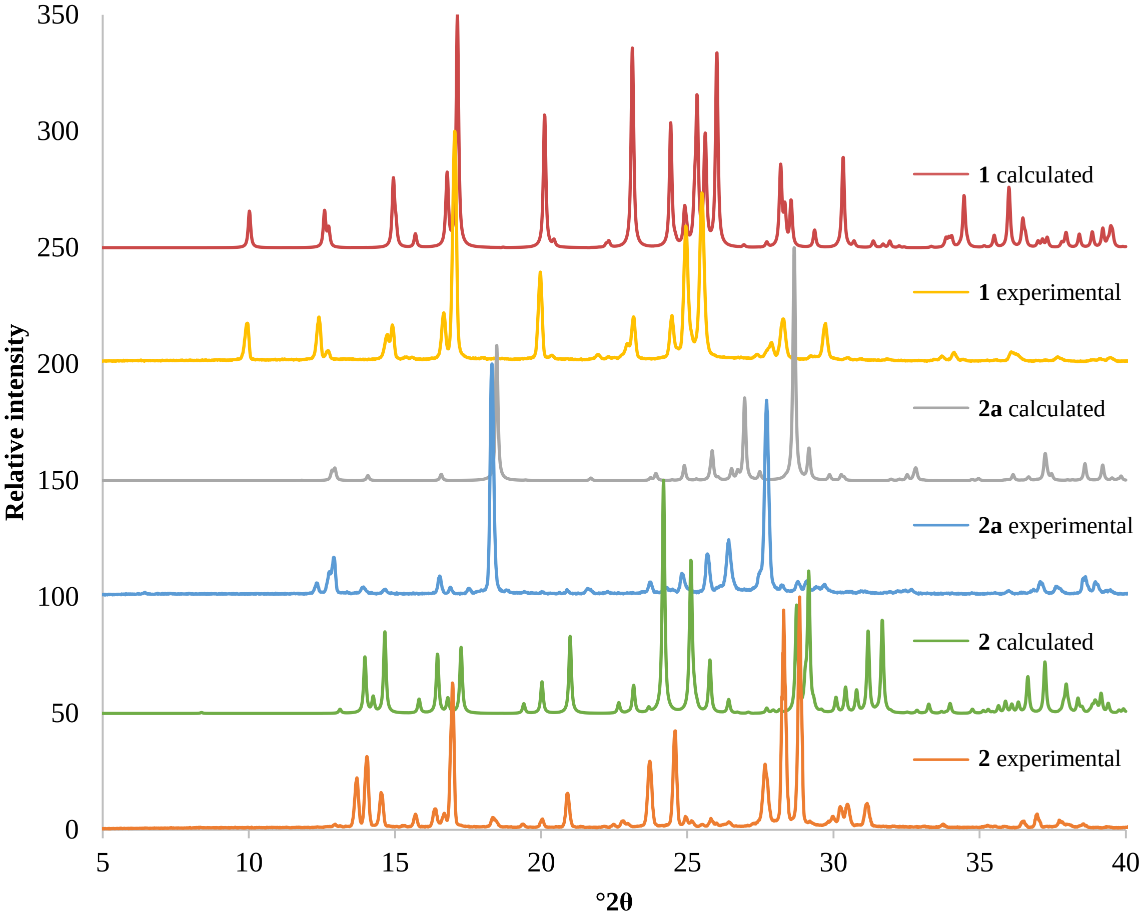

Figure S1 Comparison of the experimental and calculated powder patterns of the two zwitterions as well as the salt, **2a**. The slight shift in angle between the calculated and experimental patterns is due to the difference in temperature (powder pattern at room temperature; crystal structure at 100 K). The peak at 27.7 ° in the experimental patterns of both **2a** and **2** is due to acetylenedicarboxylic acid (starting material).

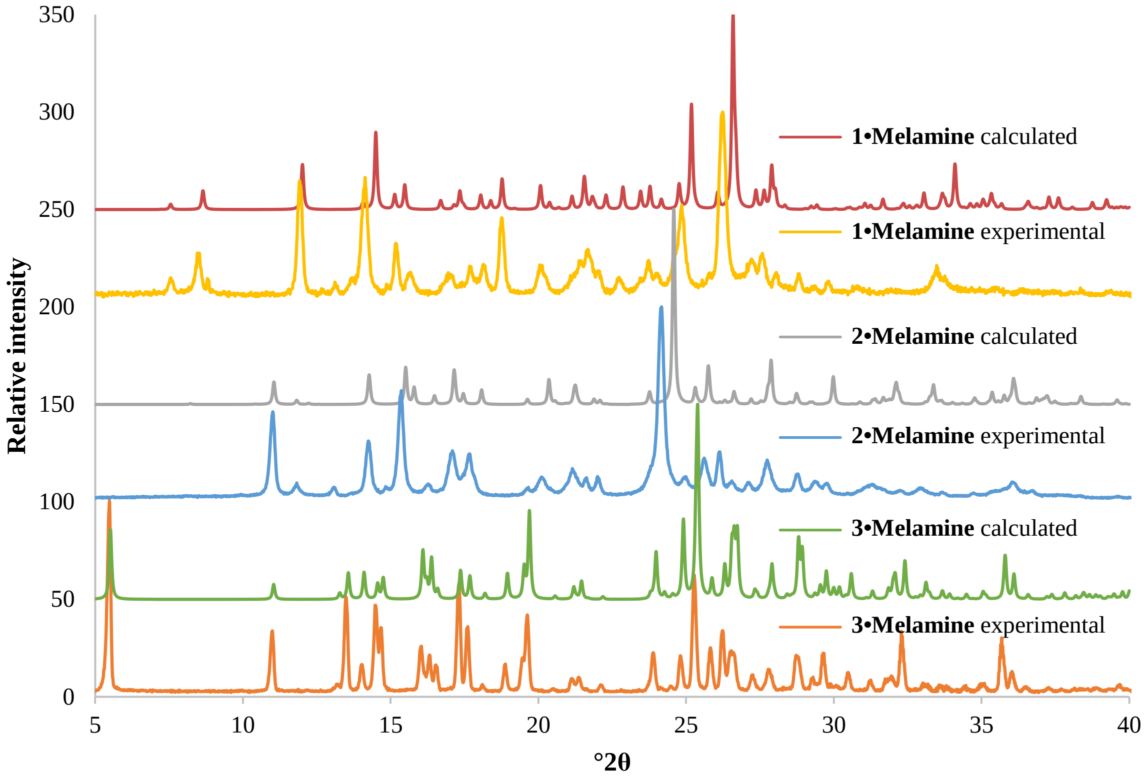

Figure S2 Comparison of the experimental and calculated powder patterns of the three melamine salts. The slight shift in angle between the calculated and experimental patterns is due to the difference in temperature (powder pattern at room temperature; crystal structure at 100 K).

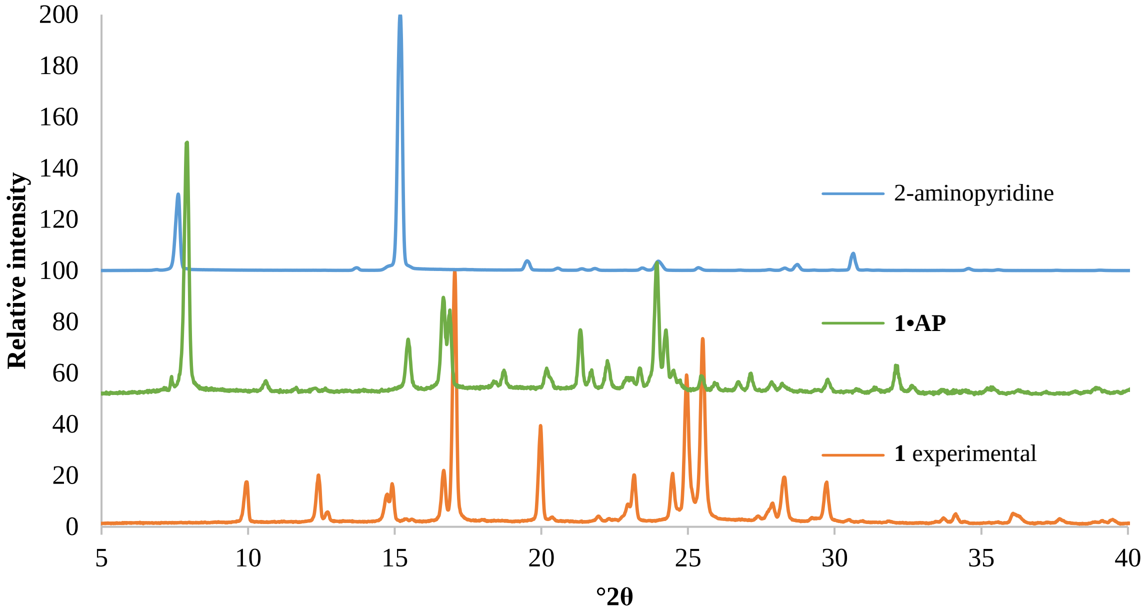

Figure S3 Comparison of the experimental powder patterns of the starting materials and the product obtained (**1•AP**) after liquid-assisted grinding (LAG) of zwitterion **1** and 2-aminopyridine with a few drops of methanol using a mortar and pestle.

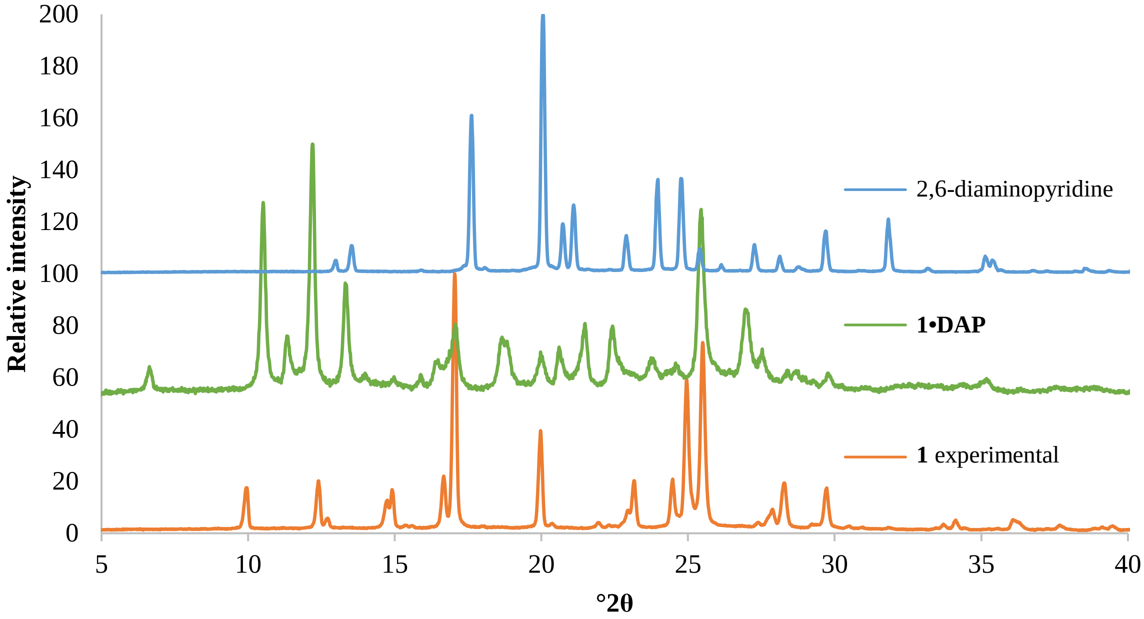

Figure S4 Comparison of the experimental powder patterns of the starting materials and the product obtained (**1•DAP**) after LAG of zwitterion **1** and 2,6-diaminopyridine with a few drops of methanol using a mortar and pestle.

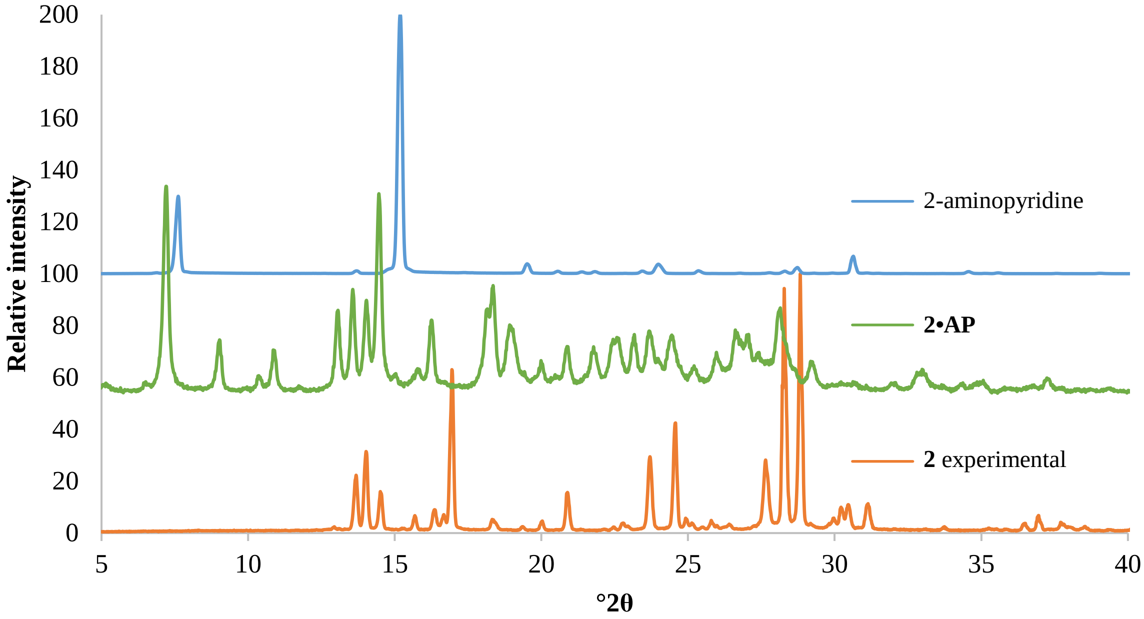

Figure S5 Comparison of the experimental powder patterns of the starting materials and the product obtained (**2•AP**) after LAG of zwitterion **2** and 2-aminopyridine with a few drops of methanol using a mortar and pestle.

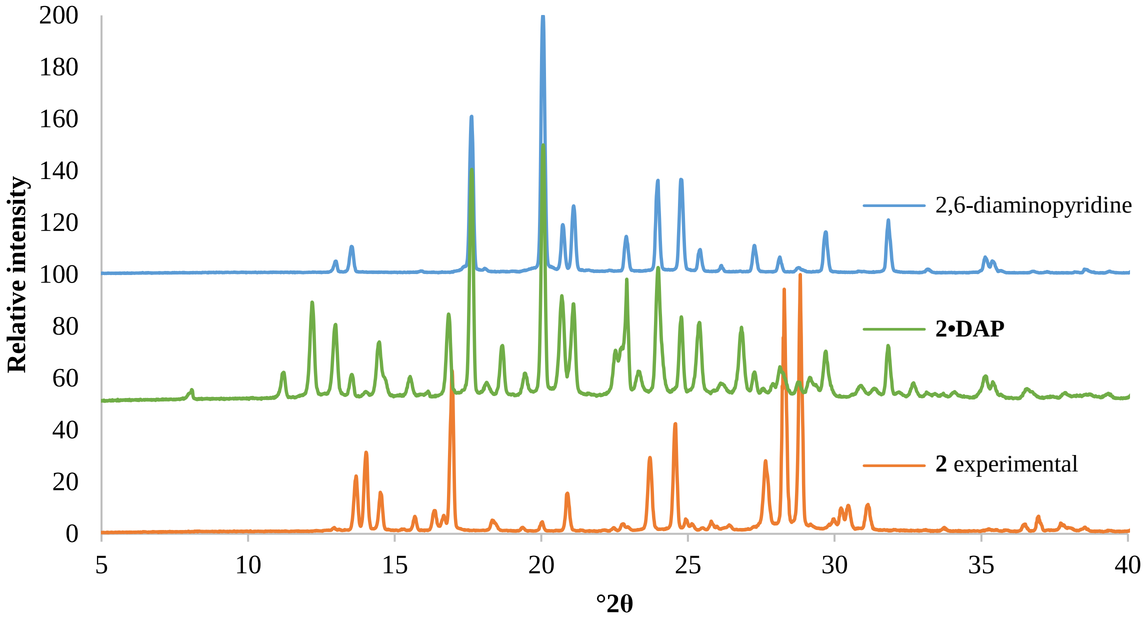

Figure S6 Comparison of the powder patterns of the starting materials and the product obtained (**2•DAP**) after LAG of zwitterion **2** and 2,6-diaminopyridine with a few drops of methanol using a mortar and pestle. Peaks of the starting materials are still visible in **2•DAP**, but new peaks have also appeared.

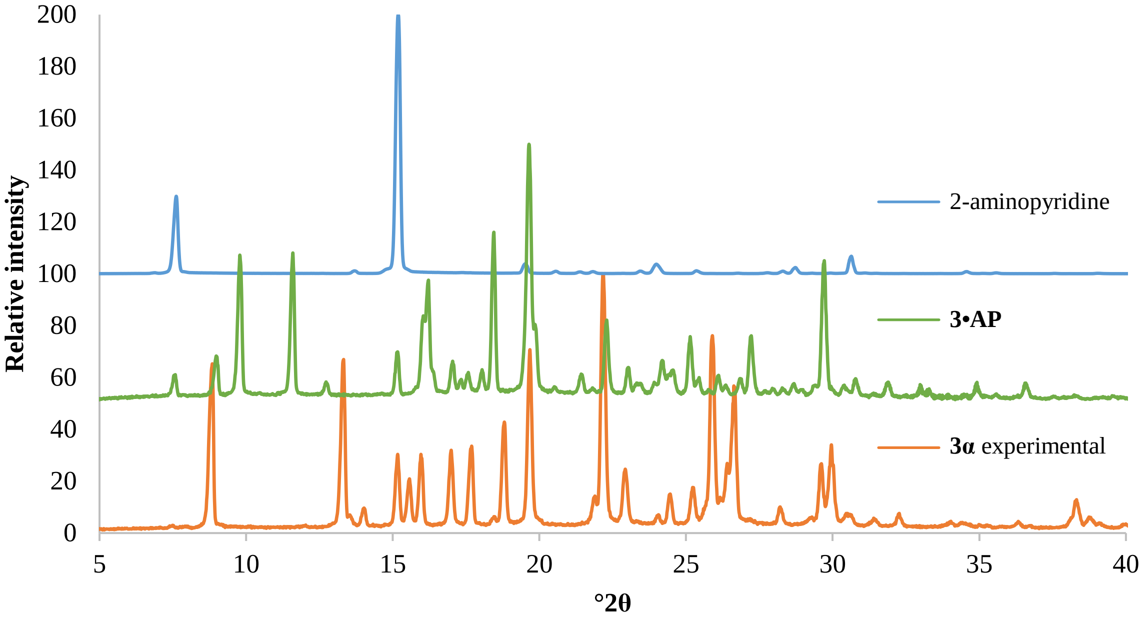

Figure S7 Comparison of the experimental powder patterns of the starting materials and the product obtained (**3•AP**) after LAG of zwitterion **3α** and 2-aminopyridine with a few drops of methanol using a mortar and pestle. Some peaks of the starting materials are still visible in **3•AP**, but new peaks have also formed.

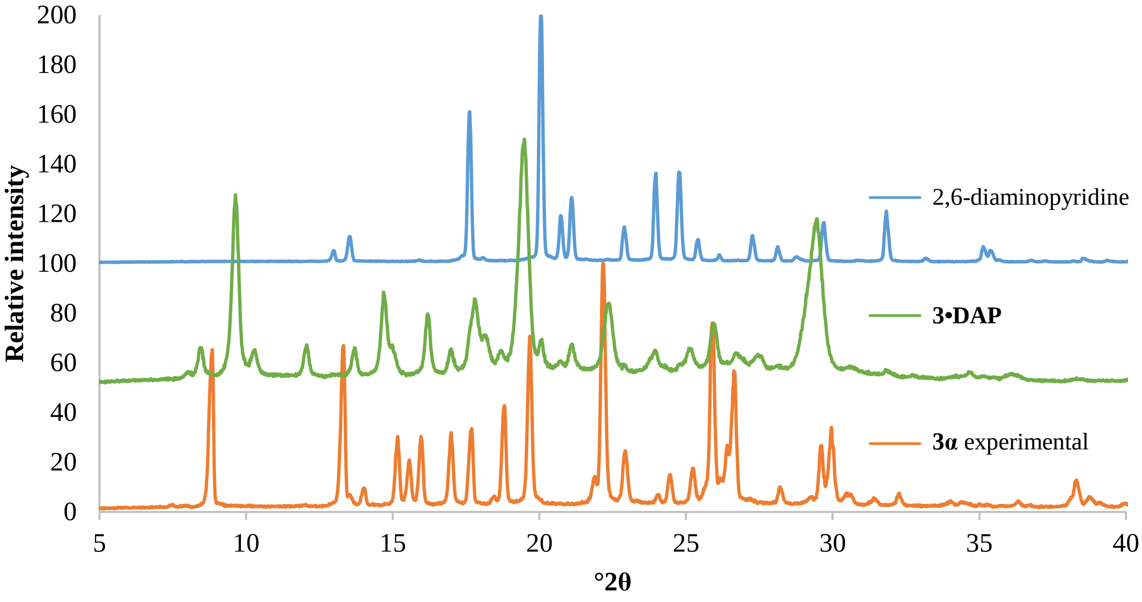

Figure S8 Comparison between the experimental powder patterns of the starting materials and the product obtained (**3•DAP**) after LAG of zwitterion **3α** and 2,6-diaminopyridine with a few drops of methanol using a mortar and pestle.

Thermal analysis (TGA and DSC)

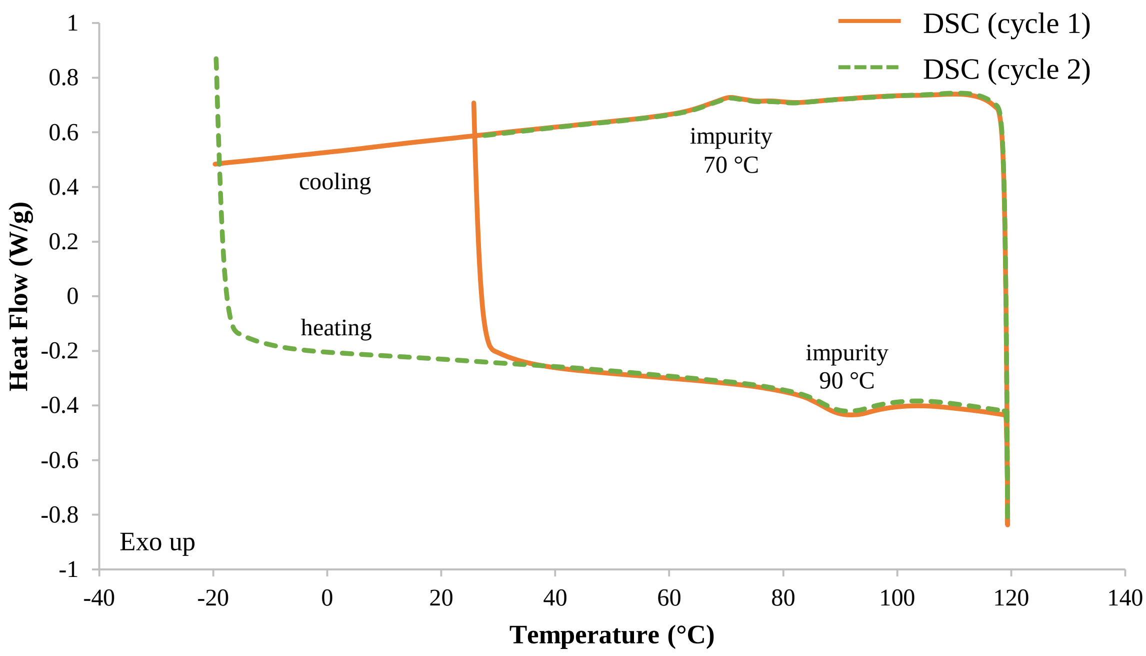

Figure S9 DSC trace for the starting material ADC. This shows the existence of an impurity in the instrument which causes the small exo- and endotherms during heating (90 °C) and cooling (70 °C). This impurity can be seen in all the following DSC curves and can be ignored (the higher the mass of the sample tested, the smaller the impurity peaks).

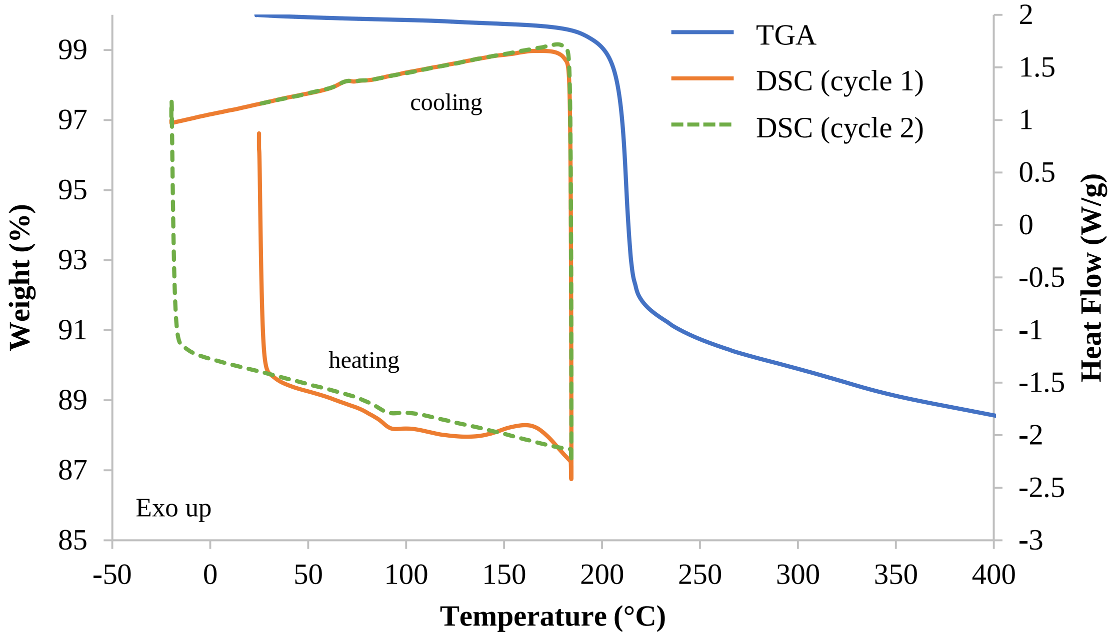

Figure S10 Thermal analysis results for zwitterion **1**. TGA trace shown in blue and DSC traces in orange (cycle 1) and green dashes (cycle 2). The small exo- and endotherms in the DSC are due to an impurity present in the instrument.

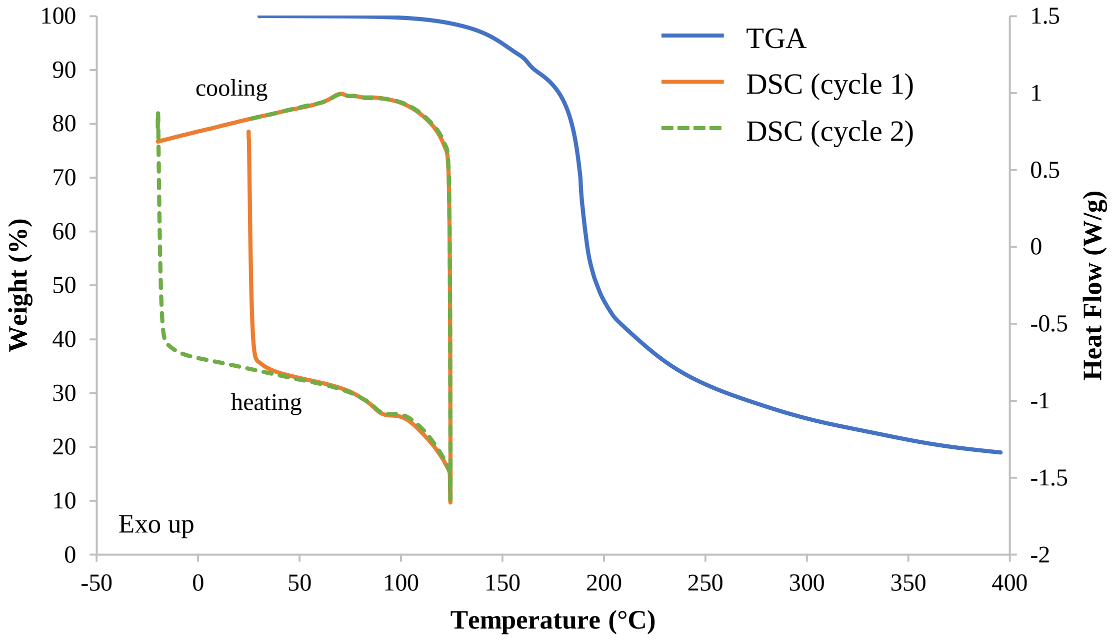

Figure S11 Thermal analysis results for zwitterion **2**. TGA trace shown in blue and DSC traces in orange (cycle 1) and green dashes (cycle 2). The small exo- and endotherms in the DSC are due to an impurity present in the instrument. The sloping baseline in the DSC trace is caused by water molecules slowly coming out of the hydrate crystals. This can also be seen in the TGA trace where there is a slow decrease in mass before degradation.

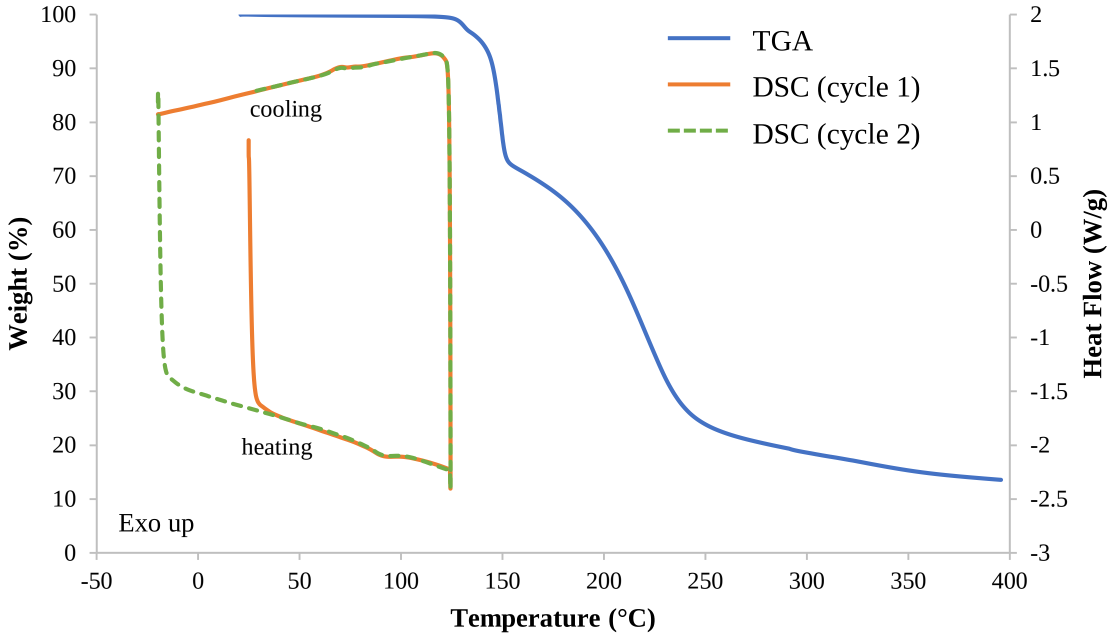

Figure S12 Thermal analysis results for the salt **2a**. TGA trace shown in blue and DSC traces in orange (cycle 1) and green dashes (cycle 2). The small exo- and endotherms in the DSC are due to an impurity present in the instrument. TGA shows a two-step degradation profile.

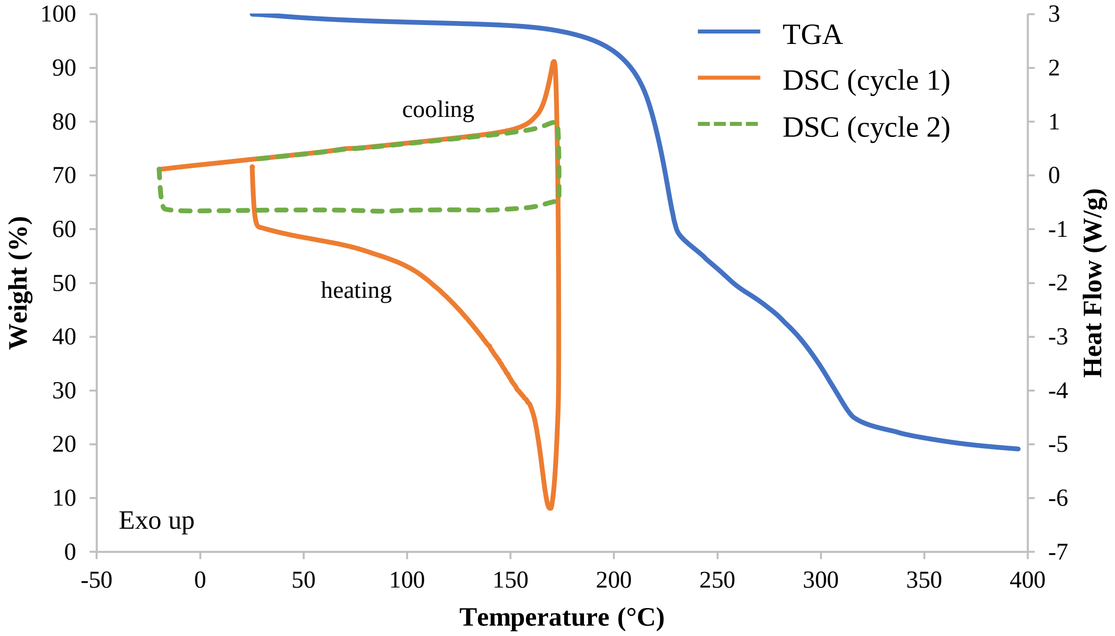

Figure S13 Thermal analysis results for the salt **1•Melamine**. TGA trace shown in blue and DSC traces in orange (cycle 1) and green dashes (cycle 2). The sloping baseline in the DSC trace is caused by water molecules slowly coming out of the hydrate crystals.

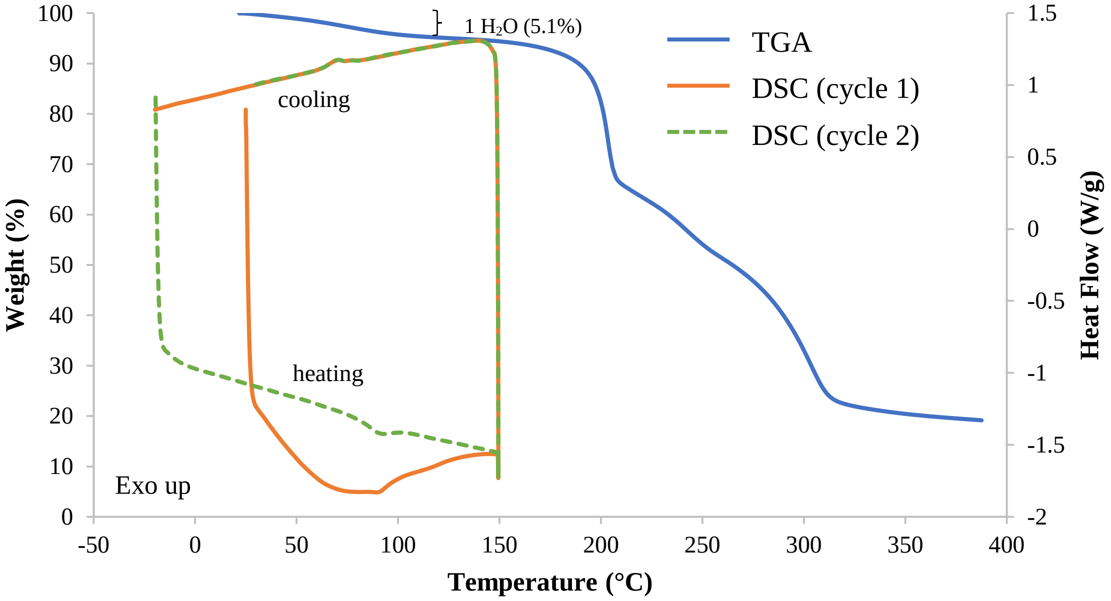

Figure S14 Thermal analysis results for salt **2•Melamine**. TGA trace shown in blue and DSC traces in orange (cycle 1) and green dashes (cycle 2). The broad endotherm in the first DSC cycle is caused by water molecules coming out of the crystals. This mass loss can also be seen in the TGA trace as a loss of 5.1%, which corresponds to the mass of one water molecule (4.8%).

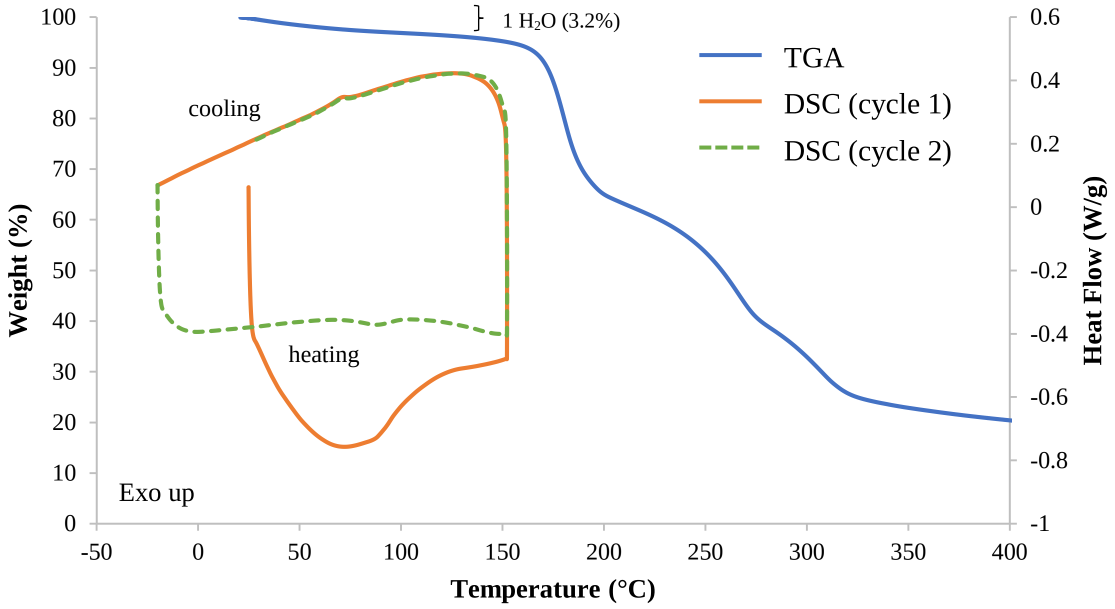

Figure S15 Thermal analysis results for salt **3•Melamine**. TGA trace shown in blue and DSC traces in orange (cycle 1) and green dashes (cycle 2). The small exo- and endotherms in the DSC are due to an impurity present in the instrument. The broad endotherm in the first DSC cycle is caused by water molecules coming out of the crystals. This mass loss can also be seen in the TGA trace as a loss of 3.2% (some water may have been lost at room temperature) that corresponds to the mass of one water molecule (calculated as 5.0%).

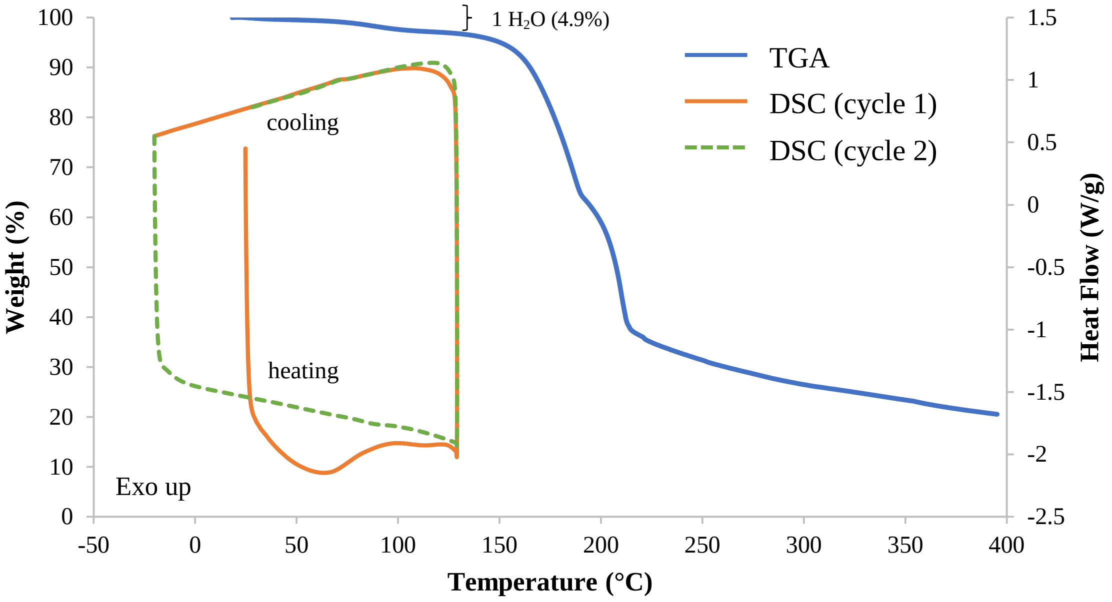

Figure S16 Thermal analysis results for the suspected salt **1•AP**. TGA trace shown in blue and DSC traces in orange (cycle 1) and green dashes (cycle 2). The endotherm in the first DSC cycle is possibly caused by solvent loss as it is not seen in the second cycle. This mass loss can also be seen in the TGA trace as a loss of 4.9%, which could indicate that this is a hydrated product (loss of one water molecule calculated as 5.2%).

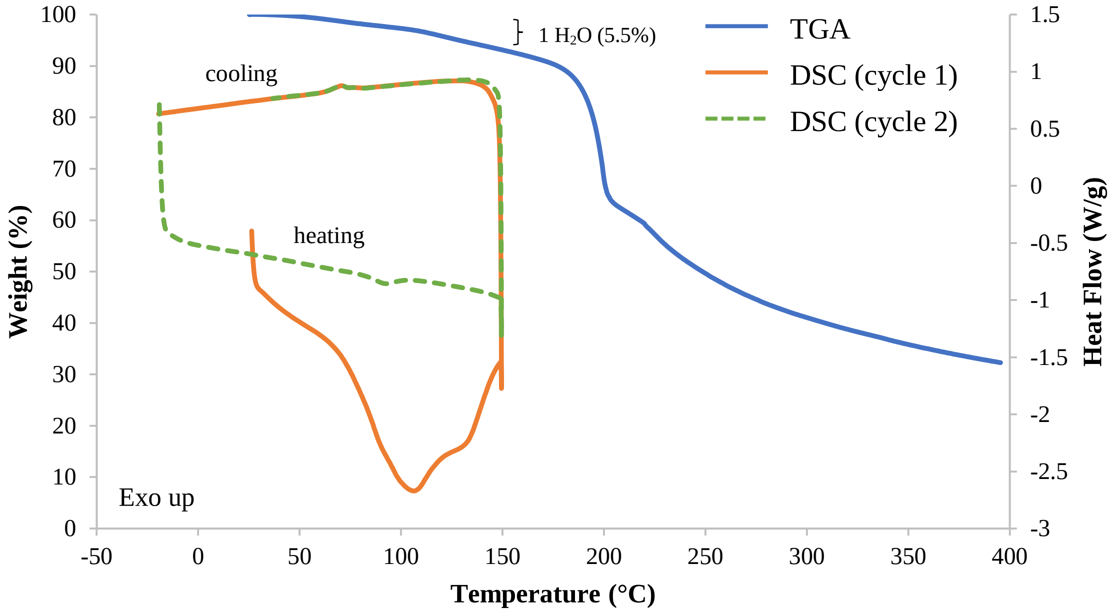

Figure S17 Thermal analysis results for the suspected salt **1•DAP**. TGA trace shown in blue and DSC traces in orange (cycle 1) and green dashes (cycle 2). The small exo- and endotherms in the DSC are due to an impurity present in the instrument. The broad endotherm in the first DSC cycle is due to slow solvent evaporation and is therefore absent in the second cycle. The TGA trace also shows a corresponding mass loss of 5.5%, which could indicate that this is a hydrated product (loss of one water molecule calculated as 5.1%.).

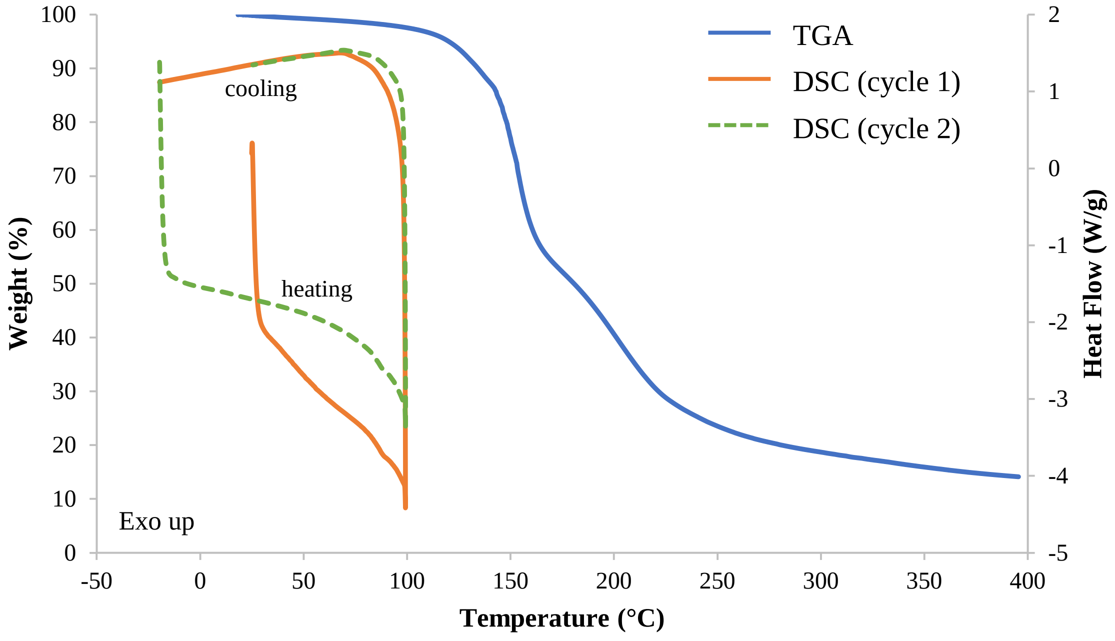

Figure S18 Thermal analysis results for the suspected salt **2•AP**. TGA trace shown in blue and DSC traces in orange (cycle 1) and green dashes (cycle 2).

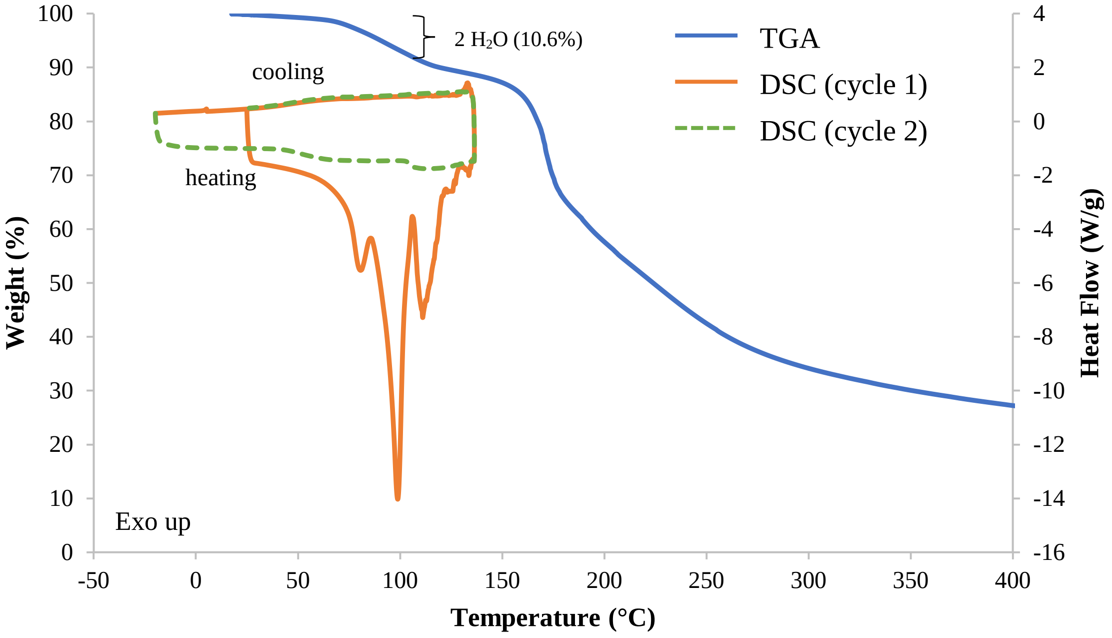

Figure S19 Thermal analysis results for the suspected salt **2•DAP**. TGA trace shown in blue and DSC traces in orange (cycle 1) and green dashes (cycle 2). The large endotherms in the first DSC cycle are due to solvent loss and are therefore absent in the second cycle. The TGA trace also shows a corresponding mass loss of 10.6%, which could indicate that this is a hydrated product (two water molecules calculated as 9.4%).

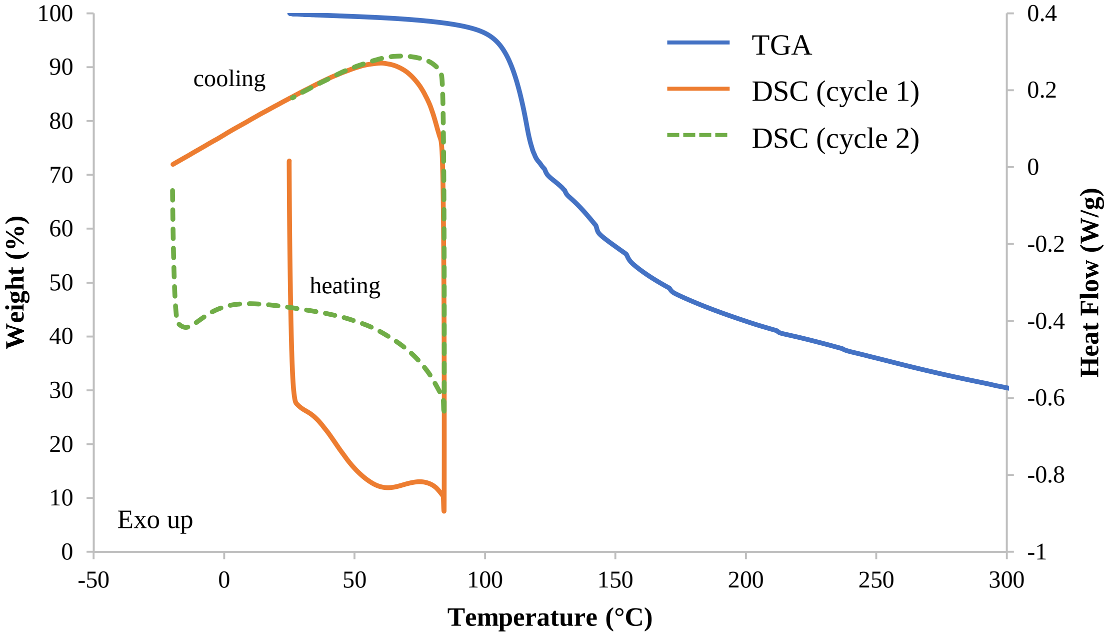

Figure S20 Thermal analysis results for the suspected salt **3•AP**. TGA trace shown in blue and DSC traces in orange (cycle 1) and green dashes (cycle 2).

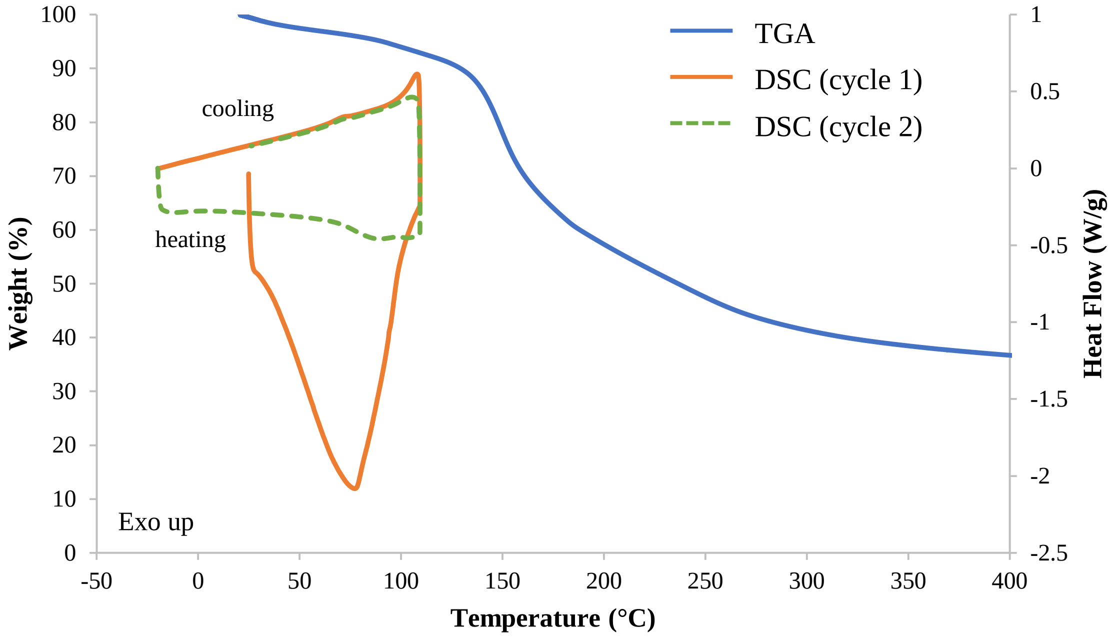

Figure S21 Thermal analysis results for the suspected salt **3•DAP**. TGA trace shown in blue and DSC traces in orange (cycle 1) and green dashes (cycle 2). The endotherm in the first DSC cycle indicates possible solvent loss. The TGA trace shows a gradual mass loss which is most likely due to water molecules being lost.

NMR

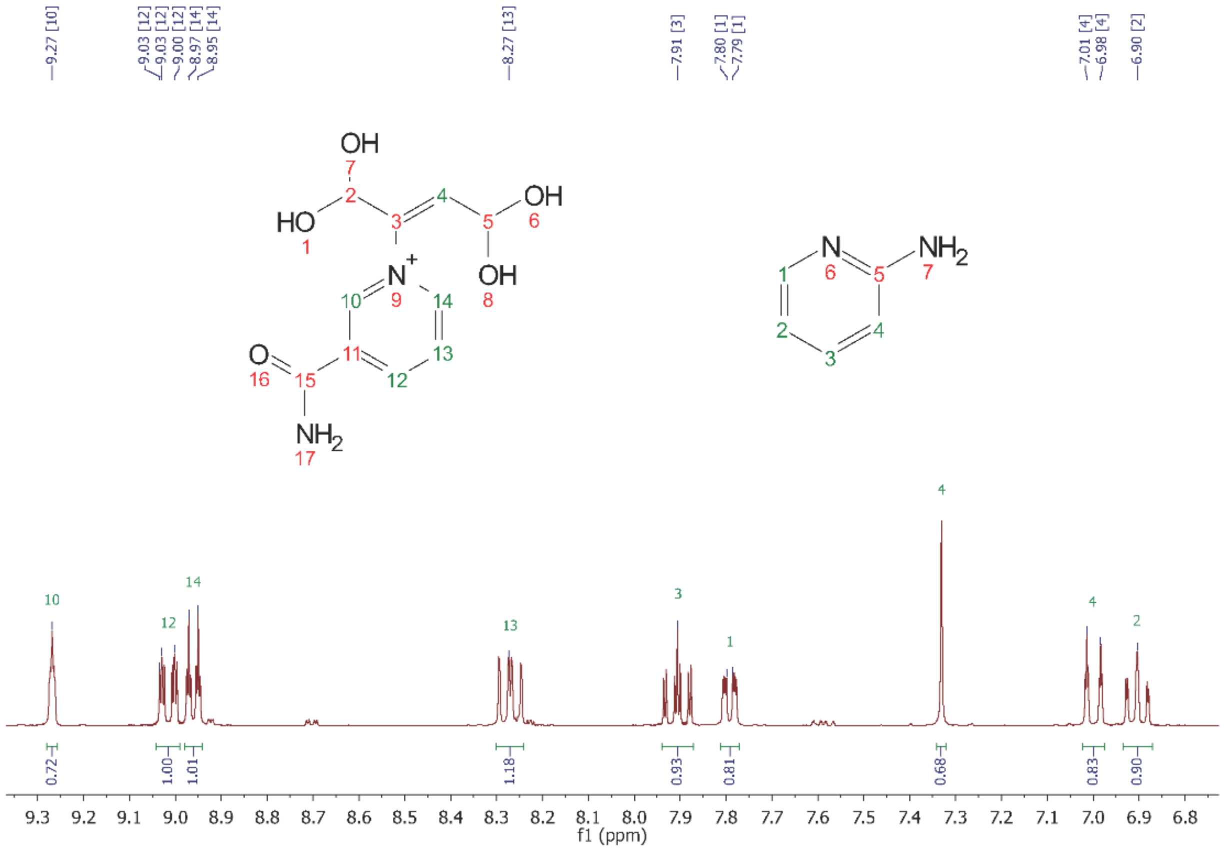

Figure S22 ^{1}H NMR spectrum (300MHz) of **1•AP** showing that both starting materials are present in the product. Peaks are referenced to the deuterium oxide peak at 4.79 ppm (not shown).

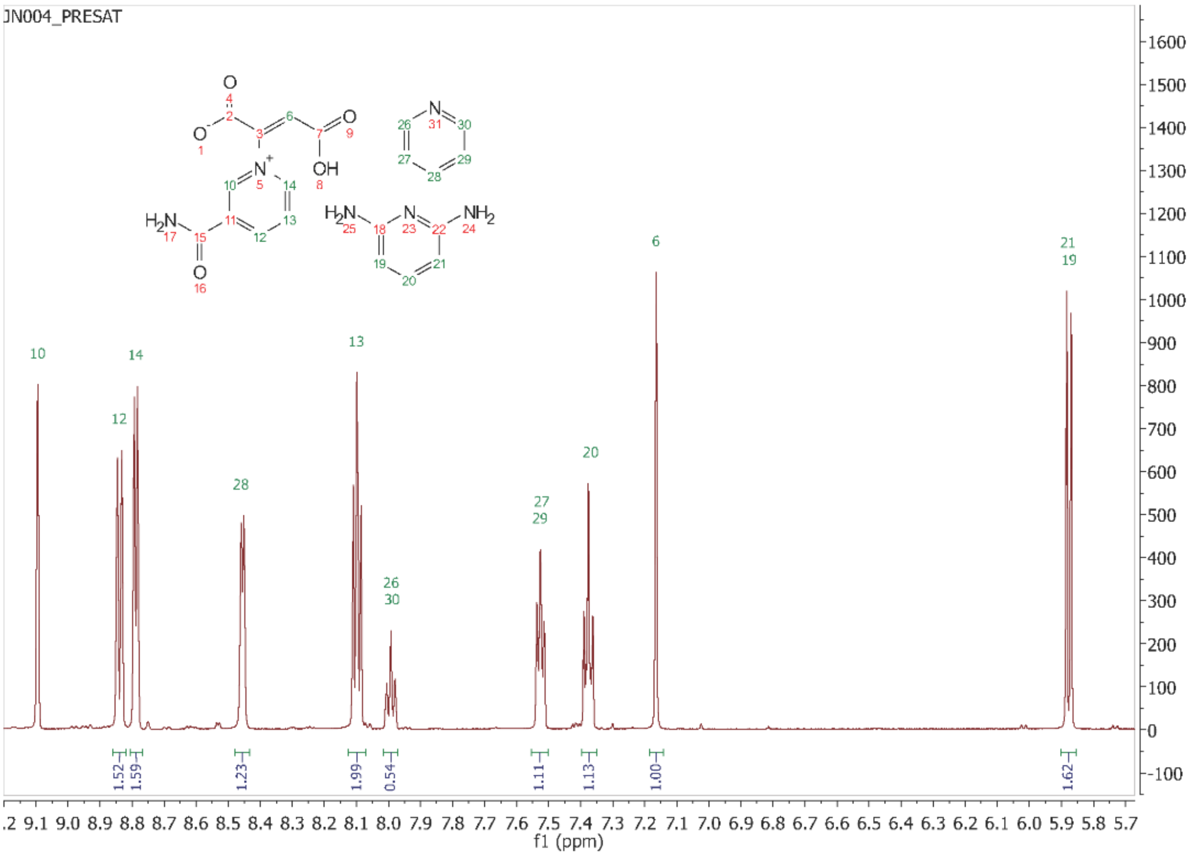

Figure S23 ^{1}H NMR spectrum (300MHz) of **1•DAP** showing that both starting materials are present in the product. A drop of pyridine was added to aid with dissolution of the sample. Peaks are referenced to the deuterium oxide peak at 4.79 ppm (not shown).

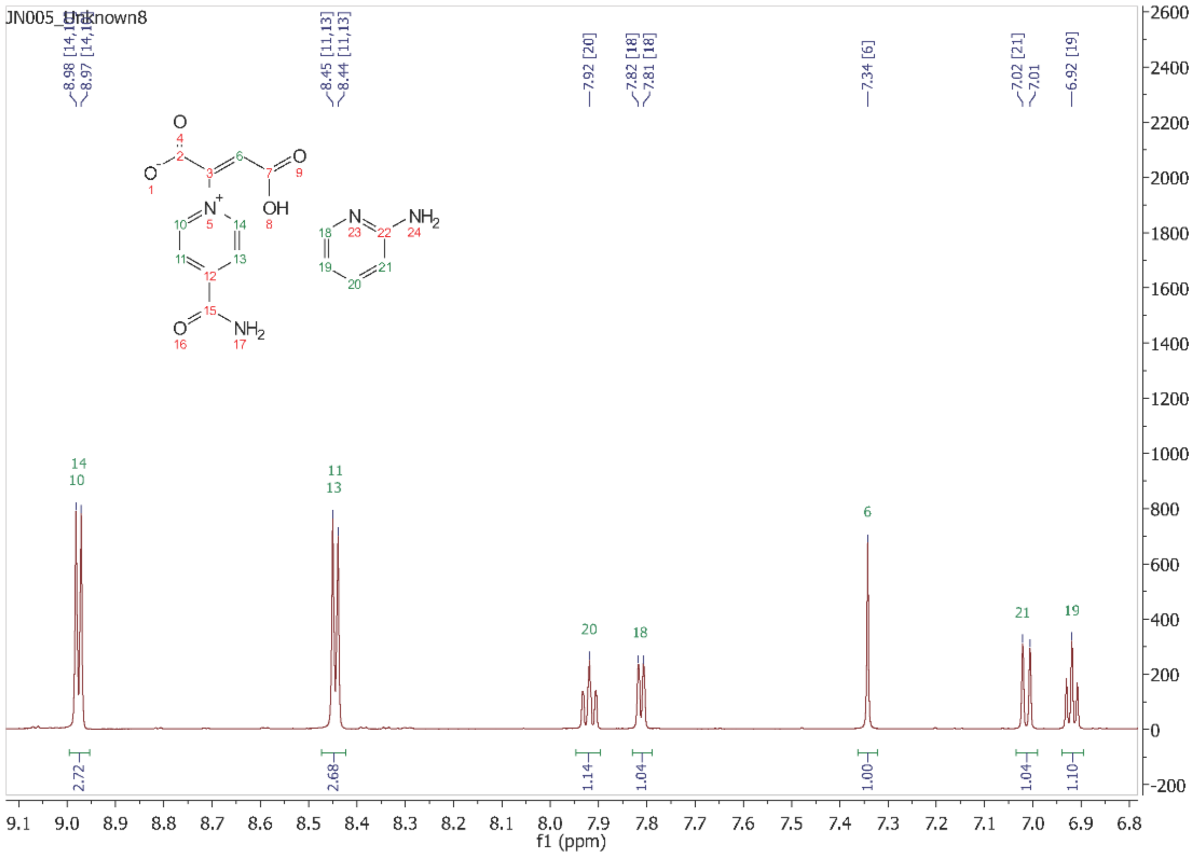

Figure S24 ^{1}H NMR spectrum (300MHz) of **2•AP** showing that both starting materials are present in the product. Peaks are referenced to the deuterium oxide peak at 4.79 ppm (not shown).

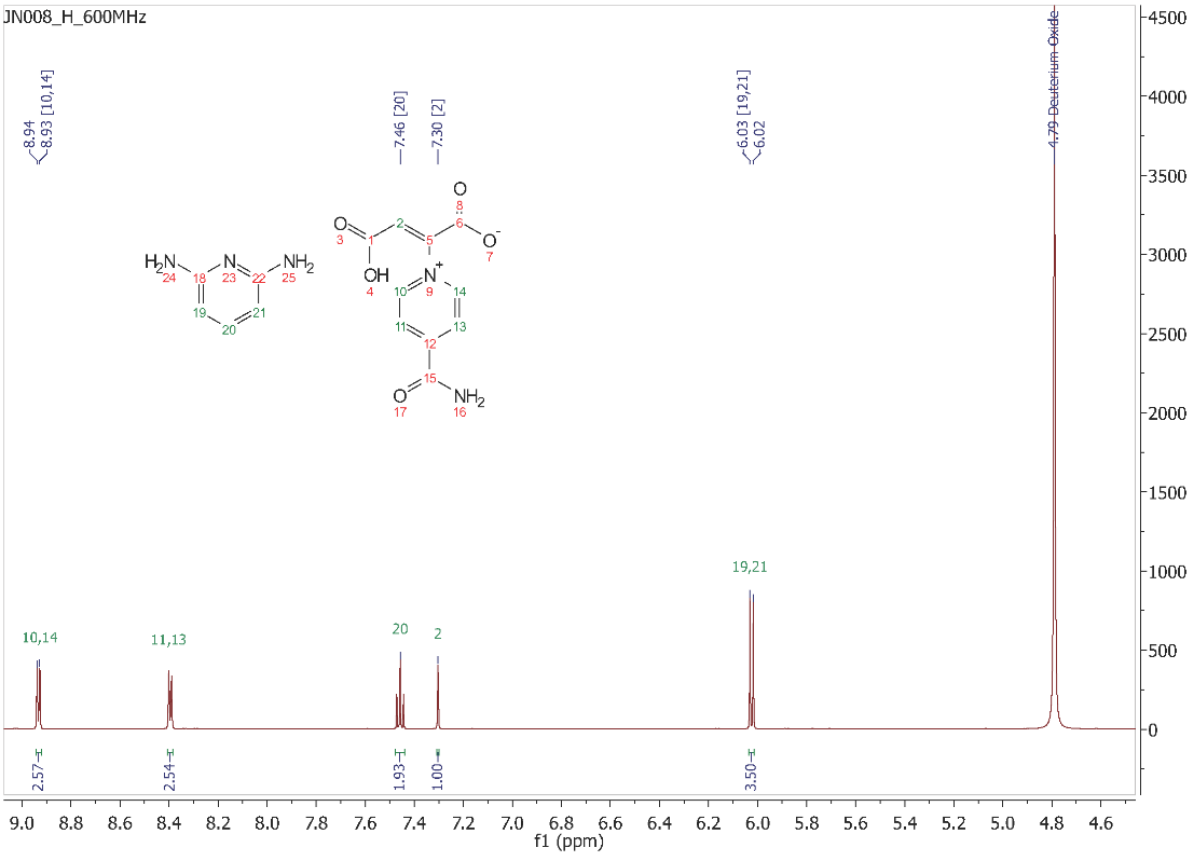

Figure S25 ^{1}H NMR spectrum (300MHz) of **2•DAP** showing that both starting materials are present in the product.

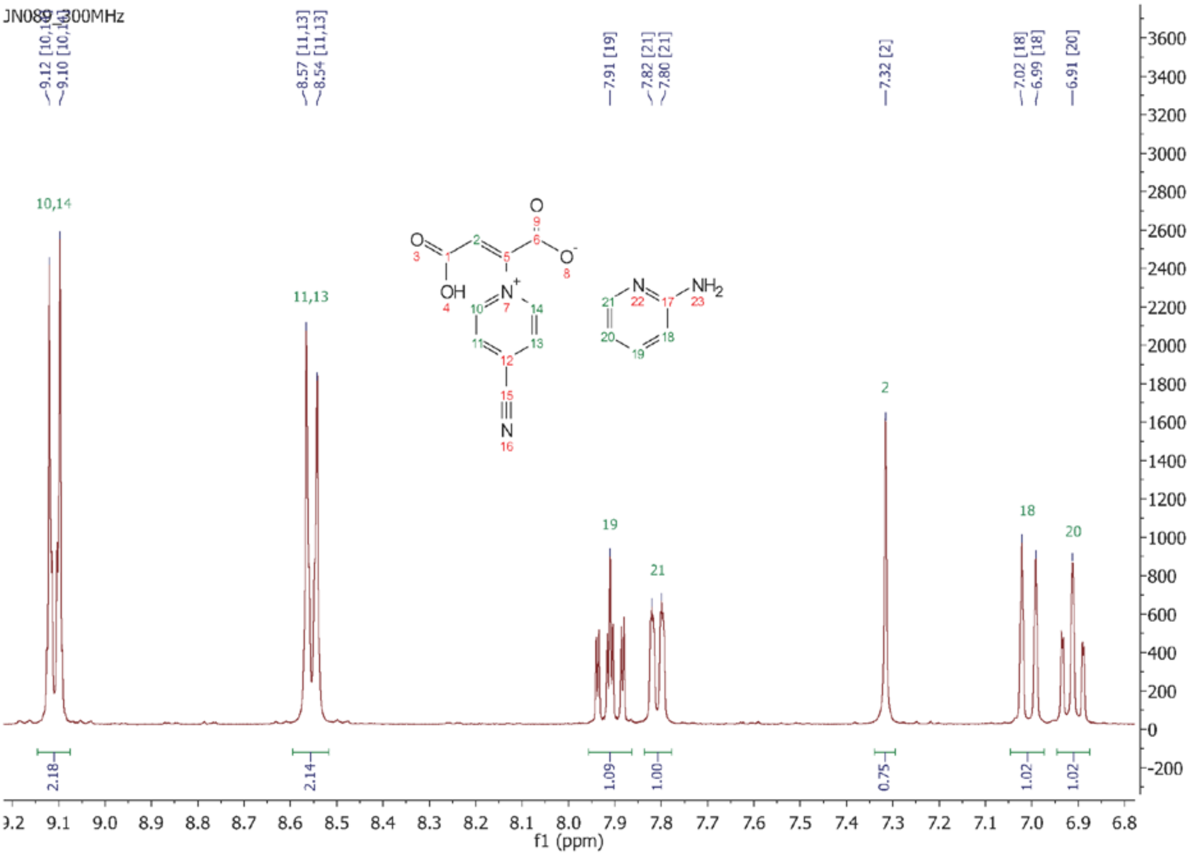

Figure S26 ^{1}H NMR spectrum (300MHz) of **3•AP** showing that both starting materials are present in the product.

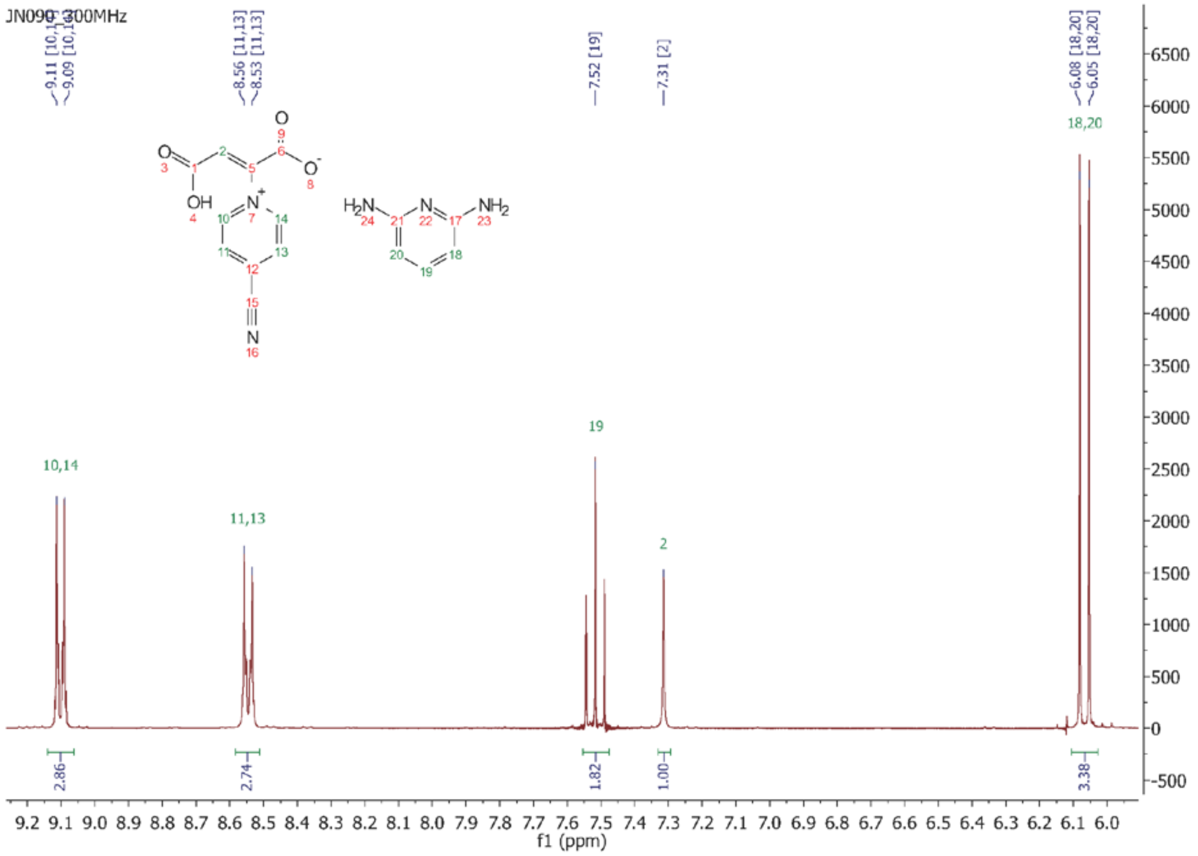

Figure S27 ^{1}H NMR spectrum (300MHz) of **3•DAP** showing that both starting materials are present in the product.

FTIR

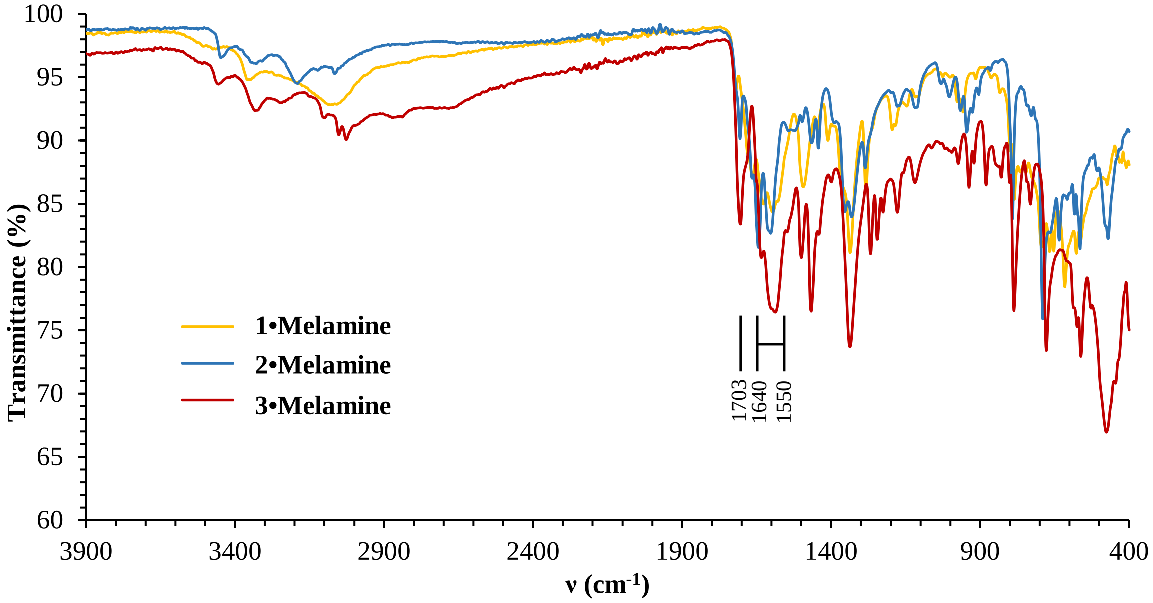

Figure S28 FTIR spectra for the three melamine salts, **1•Melamine**, **2•Melamine**, and **3•Melamine**. The region from 1550-1640 cm^{-1} represents the carboxylate C=O stretching frequencies. The weaker peaks at 1703 cm^{-1} indicate that the hydrogen atom is slightly disordered between the nitrogen and oxygen atom to give the materials a slight co-crystal character, although they are still predominantly salts.

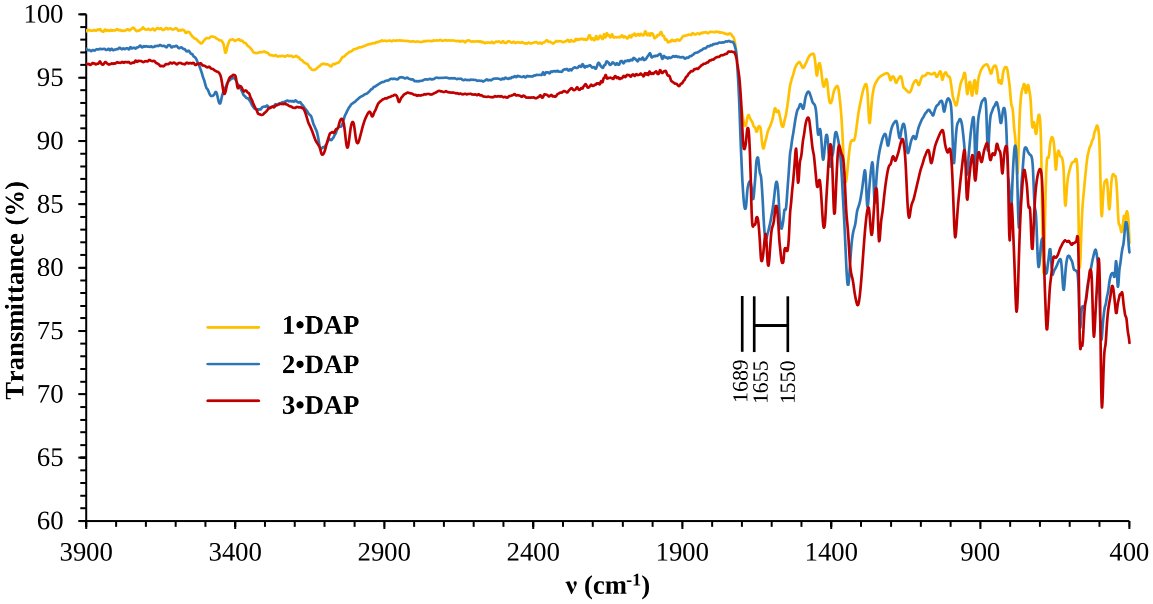

Figure S29 FTIR spectra for the three suspected 2,6-diaminopyridine salts, **1•DAP**, **2•DAP**, and **3•DAP**. The region from 1550-1655 cm^{-1} represents the carboxylate C=O stretching frequencies. The weaker peaks at 1689 cm^{-1} indicate that the hydrogen atom is slightly disordered between the nitrogen and oxygen atom to give the materials a slight co-crystal character, although they are still predominantly salts.

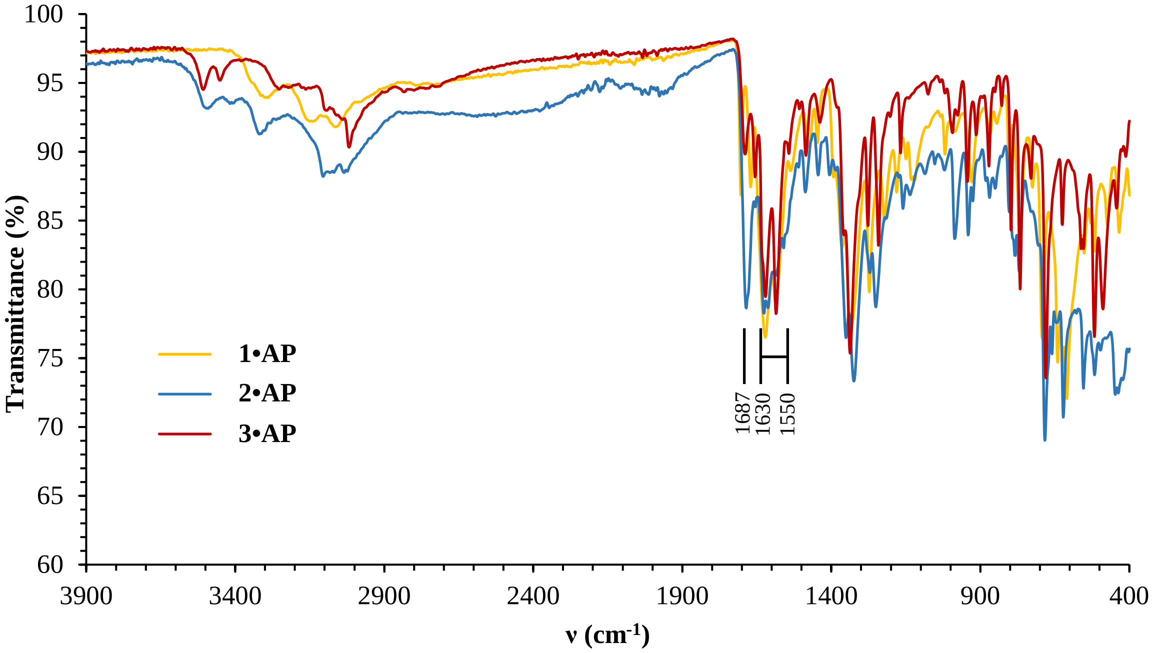

Figure S30 FTIR spectra for the three suspected 2-aminopyridine salts, **1•AP**, **2•AP**, and **3•AP**. The region from 1550-1630 cm^{-1} represents the carboxylate C=O stretching frequencies. The weaker peaks at 1687 cm^{-1} indicate that the hydrogen atom is slightly disordered between the nitrogen and oxygen atom to give the materials a slight co-crystal character, although they are still predominantly salts.